Magnetism and hyperfine fields in melt-spun R-Fe-B alloys with a low R concentration (R identical to Y, Pr, Nd, Gd or Dy)

1995 J. Phys.: Condens. Matter 7 2303

(http://iopscience.iop.org/0953-8984/7/11/008)

J. Phys.: Condens. Matter 7 (1995) 2303–2312. Printed in the UK

Magnetism and hyperfine fields in melt-spun R–Fe–B alloys with a low R concentration (R ≡ Y, Pr, Nd, Gd or Dy)

Zhao-hua Cheng†‡, Ming-xi Mao‡ Ji-jun Sun‡, Bao-gen Shen†, Fang-wei Wang†, Chun-li Yang‡, Yi-de Zhang‡ and Fa-shen Li‡

† State Key Laboratory of Magnetism, Institute of Physics, Chinese Academy of Sciences, Beijing 100 080, People's Republic of China

‡ Department of Physics, Lanzhou University, Lanzhou 730000, People's Republic of China

Received 8 November 1994

Abstract. The hyperfine fields and magnetic properties of amorphous and crystallized $R_xNd_{4-x}Fe_{77.5}B_{18.5}$ (R ≡ Y, Pr, Gd or Dy; $0 \leqslant x \leqslant 4$) alloys have been investigated by means of magnetization measurements, zero-field spin-echo nuclear magnetic resonance (NMR) and the Mössbauer effect (ME). It is found that the Curie temperatures of amorphous alloys change slightly on the addition of R, but the coercive fields of crystallized alloys decrease monotonically with increasing x for R ≡ Y, Pr and Gd. A small addition of Dy increases the coercivity; full substitution of Nd by Dy leads to low coercivity owing to the formation of the magnetically soft $Dy_3Fe_{62}B_{14}$. NMR, ME and x-ray diffraction indicate that the samples with R ≡ Pr and Gd for $0 \leqslant x \leqslant 4$ and R ≡ Y and Dy for $0 \leqslant x \leqslant 2$ consist of Fe_3B with a body-centred tetragonal (BCT) structure and a small amount of α-Fe. Furthermore, the NMR results indicate that the ^{11}B hyperfine fields of BCT Fe_3B increase linearly from 25.3 kOe (34.7 MHz) to 26.3 kOe (36.0 MHz) on the addition of Dy or Gd, but that of α-Fe does not change with increasing R concentration; the Mössbauer spectra show that the relative intensity of the subspectrum corresponding to ^{57}Fe at $Fe_{II}(8g)$ sites in BCT Fe_3B is about 5% weaker than those of the other two, implying that about 5 at.% Fe atoms in this site are substituted by other atoms. According to this, it may be reasonable to assume that R atoms enter into BCT Fe_3B.

1. Introduction

Since the discovery of the new melt-spun R–Fe–B permanent magnetic materials containing Fe_3B as the main phase, many experimental studies have been reported on the magnetic properties and crystallization products of these compounds [1–6]. It was found that $Nd_4Fe_{77.5}B_{18.5}$ melt-spun ribbons showed a coercivity of 3 kOe, a magnetic remanence of 12.5 kG and an energy product of 13 MG Oe at room temperature after appropriate heat treatments [6]. Although the rare-earth Nd concentration in this sample is only about one third of that in crystallized Nd–Fe–B with 12–16 at.% Nd, their maximum energy product $(BH)_{max}$ are about the same and the remanence magnetization of the former is even higher. Thus, it can be used as an inexpensively bonded permanent magnet. The main application is expected in devices in which the demagnetizing field is low, because of the relatively low coercive field H_c. However, until now, the origin of the hard magnetic properties has not been clarified.

Previous work assumed that the hard magnetic properties originated from the existence of a $Nd_2Fe_{14}B$ hard magnetic phase on the basis of magnetic phase analysis, but there is a lack of direct evidence. One point of view assumes that atomic ordering in the $Nd_2Fe_{14}B$

0953-8984/95/112303+10$19.50

lattice may still be far from perfect and its grain size is too small to be resolved by x-ray diffraction (XRD). It is known that XRD is only sensitive to a well developed phase while both nuclear magnetic resonance (NMR) and the Mössbauer effect (ME) can provide local information concerning the nearest-neighbour environment of the detected nuclei. Thus, both of these can be employed to identify the phase composition whose dimensions are too small for XRD techniques. Recently, NMR and ME results demonstrated that the $Nd_2Fe_{14}B$ hard magnetic phase was not present in these samples [7, 8]. Furthermore, NMR indicated that the ^{11}B spectrum corresponding to Fe_3B with a body-centred tetragonal (BCT) structure broadened asymmetrically to the high-frequency side; the ME spectrum showed that the relative intensity of the third subspectrum corresponding to the $Fe_{III}(8g)$ site in BCT Fe_3B is about 5 at.% weaker than those of others. These facts implied that Nd atoms enter into the BCT Fe_3B lattice. In this paper, we present a combined NMR and ME study to investigate the effect of substitution of Nd by some rare-earth elements, including Y, on the magnetic properties, phase components and hyperfine fields of melt-spun Nd–Fe–B with a few per cent of Nd.

2. Experimental details

Raw materials of iron (purity 99.9%), rare-earth metal R (R ≡ Y, Pr, Nd, Gd or Dy; purity, 99.9%) and Fe–B alloys (purity 98.6%) were arc melted into homogeneous buttons with the nominal composition $Nd_{4-x}R_xFe_{77.5}B_{18.5}$ (R ≡ Y, Pr, Gd or Dy; $0 \leqslant x \leqslant 4$). Amorphous ribbons were prepared by melt spinning in a high-purity argon atmosphere at a speed of 47 m s^{-1}. The thickness and width of the ribbons were about 20 μm and 1 mm, respectively. XRD patterns confirmed the amorphous state of the ribbons. The Curie temperatures T_C of these amorphous alloys were determined by the temperature dependence of the AC susceptibility in a very weak magnetic field, less than 1 Oe. The as-quenched ribbons were annealed at 670 °C for about 10 min in steel capsules evacuated to 2×10^{-5} Torr. Hysteresis loop measurements on the heat-treated samples were carried out at room temperature using vibrating-sample magnetometer with a maximum magnetic field of 8 kOe. The magnetization curves at 1.5 K were measured by means of an extracting-sample magnetometer with a magnetic field range 0–70 kOe. The saturation magnetization was obtained from fitting the experimental data of $M(H)$ versus H using the law of approach to saturation.

Zero-field spin-echo NMR spectra of ^{11}B and ^{57}Fe were performed at a temperature of 8 K for frequencies ranging from 20 to 60 MHz. A closed-cycle refrigerator was employed to provide this low temperature without the consumption of liquid helium. The details of NMR experiments have been described elsewhere [8]. The Mössbauer spectra were recorded at room temperature using a constant-acceleration spectrometer with a $^{57}Co(Pd)$ source. The isomer shifts given in this paper were relative to α-Fe at room temperature. The XRD experiments were performed with Co Kα radiation.

3. Results and discussion

Figure 1 shows the ^{11}B NMR spectrum of the amorphous alloy $Nd_4Fe_{77.5}B_{18.5}$. The very wide spectrum demonstrates a typical amorphous pattern. The resonance line shows two peaks centred at 34.7 and 36.3 MHz. According to our previous NMR study on Fe–B–C amorphous alloys [9], these two peaks are attributed to BCT-Fe_3B-like and orthorhombic

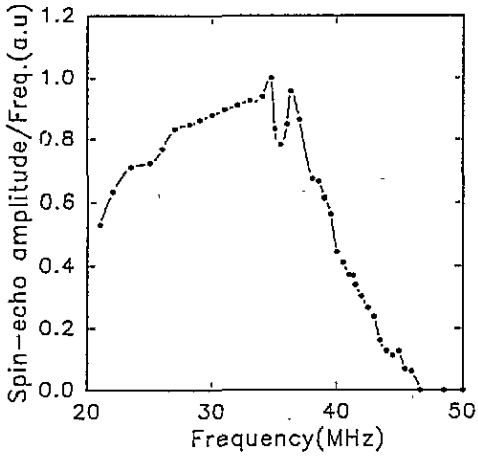

Figure 1. Spin-echo NMR spectrum of $Nd_4Fe_{77.5}B_{18.5}$ amorphous alloy (a.u., arbitrary units).

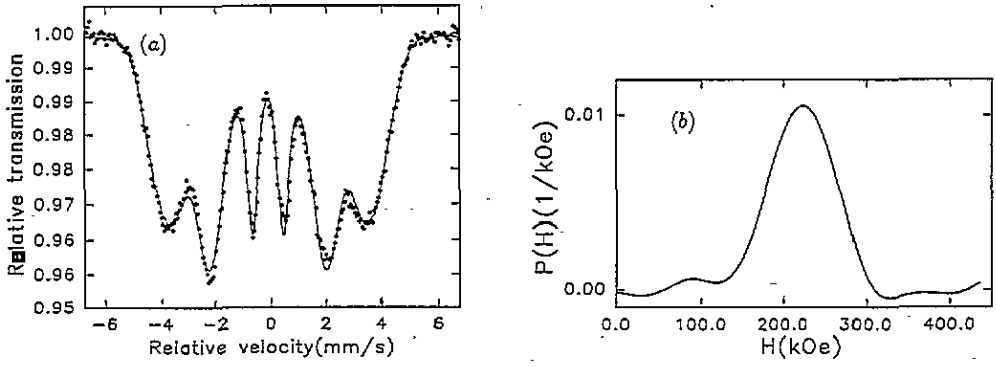

Figure 2. ^{57}Fe Mössbauer spectrum and hyperfine field distribution $P(H)$ versus H for $Nd_4Fe_{77.5}B_{18.5}$ amorphous alloy.

Fe_3B-like short-range order, respectively. The Mössbauer spectrum of amorphous ribbon is a typical amorphous broad sextet with a peak hyperfine field of 225 kOe and an average of 218 kOe (figure 2(b)). However, the broad sextet, corresponding to one wide peak of the hyperfine field distribution $P(H)$, cannot directly provide information concerning the types of short-range order. This provides evidence that the types of short-range order can be investigated by NMR more directly than by ME. The average hyperfine fields at ^{11}B and ^{57}Fe in this amorphous alloy are smaller than in $Fe_{80}B_{20}$ amorphous alloy [10]. The substitution of R is found to have no obvious effect on the types of short-range order in amorphous alloys with a few per cent R.

Figure 3 shows the variation in Curie temperatures for $R_xNd_{4-x}Fe_{77.5}B_{18.5}$ amorphous alloys with R concentration. It is found that the Curie temperature increases slightly for R ≡ Gd or decreases slightly for R ≡ Y, Pr and Dy, with increasing x. For rare-earth–iron compounds or alloys, the Curie temperature is determined by Fe–Fe, R–Fe and R–R exchange interactions. It is commonly assumed that the Fe–Fe exchange interaction plays a predominant role and the R–R interaction can be negligible in iron-rich compounds. This assumption is supported by the fact that the substitution of R has no obvious effect on the Curie temperatures of R–Fe–B amorphous alloys. The variation in T_C for different rare-

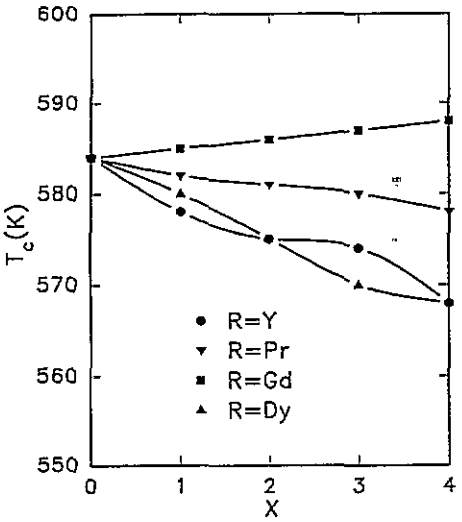

Figure 3. Curie temperature of amorphous $R_xNd_{4-x}Fe_{77.5}B_{18.5}$ alloys as a function of R concentration x.

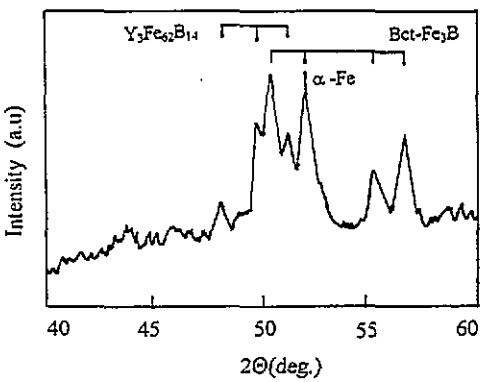

Figure 4. XRD pattern of $Y_4Fe_{77.5}B_{18.5}$ alloy annealed at 670 °C.

earth compounds is mainly attributed to the effect of R–Fe interaction on T_C. The R–Fe interaction is proportional to the de Gennes factor $(g-1)^2J(J+1)$ for rare-earth ions on the basis of molecular-field theory. The increase or decrease in T_C with increasing x is mainly determined by the de Gennes factor of the R ion which is greater or less than that of the Nd ion.

Table 1. The magnetic parameters of $R_4Fe_{77.5}B_{18.5}$ amorphous alloys.

R	$\sigma_s(1.5)$ (A m^2 kg^{-1})	$\bar{\mu}_{Fe}$ (μ_B)	$\bar{\mu}_R$ (μ_B)	gJ (μ_B)	T_C (K)
Y	171	1.93	0	0	568
Pr	175	1.93	2.54	3.2	578
Nd	174	1.93	2.37	3.27	584
Gd	132	1.93	7.0	7.0	588
Dy	123	1.93	8.9	10.0	568

The saturation magnetizations of amorphous alloys $R_4Fe_{77.5}B_{18.5}$ are listed in table 1. The average iron moment $\bar{\mu}_{Fe}$ can be obtained from $Y_4Fe_{77.5}B_{18.5}$ amorphous alloy. If we assume that the average iron moment $\bar{\mu}_{Fe}$ is constant for all samples and that there is a collinear structure between Fe and R moments, the average rare-earth moments $\bar{\mu}_R$ can be derived from the formula:

$$\bar{\mu}_M = \sigma_s(0)/(N\mu_B) \tag{1}$$

$$\bar{\mu}_M = 77.5\bar{\mu}_{Fe} + 4\bar{\mu}_R \tag{2}$$

for R ≡ light rare-earth elements and

$$\mu_M = 77.5\bar{\mu}_{Fe} - 4\bar{\mu}_R \tag{3}$$

for R ≡ heavy rare-earth elements, where N is Avogadro's number, μ_B is the Bohr magneton and M is the molecular weight of $R_4Fe_{77.5}B_{18.5}$ alloys. The value of $\sigma_s(0)$ at 0 K is very close to that of $\sigma_s(1.5)$ at 1.5 K; thus, we can use $\sigma_s(1.5)$ to replace $\sigma_s(0)$.

These values are also summarized in table 1. It can be found that the rare-earth moments μ_R are much less than those of the free R^{3+} ion, which implies that there is a non-collinear structure between R and Fe moments for R ≡ Pr, Nd and Dy. This phenomenon was also observed in R–TM amorphous films [11] and $(Fe_{1-x}Nd_x)_{81.5}B_{18.5}$ amorphous alloys [12].

XRD results demonstrate that the addition of Pr and Gd does not change the phase composition when the samples are annealed at 670 °C for a short time, while the full substitution of Nd by Y or Dy will change the phase composition. A new metastable phase $R_3Fe_{62}B_{14}$ will appear in the annealed samples with $x > 2$. For example, figure 4 illustrates the XRD pattern of $Y_4Fe_{77.5}B_{18.5}$ alloy annealed at 670 °C. The pattern shows that, in addition to BCT Fe_3B and α-Fe, a new phase $Y_3Fe_{62}B_{14}$ is present in this sample. A previous study demonstrated that this magnetic phase had a cubic structure with a lattice constant $a = 12.35$ Å [13].

The Mössbauer spectra of $R_4Fe_{77.5}B_{18.5}$ alloys annealed at 670 °C were best fitted with four subspectra for R ≡ Pr, Nd and Gd (figures 5(a)–(c)). The subspectrum with a hyperfine field of 331 kOe corresponds to α-Fe; the others are attributed to ^{57}Fe in the three iron sites of BCT Fe_3B. The substitution of R for Nd has no obvious influence on ^{57}Fe hyperfine fields in BCT Fe_3B. However, the Mössbauer spectra indicate that the relative intensity of the third subspectrum corresponding to the $Fe_{III}(8g)$ site of BCT Fe_3B is about 5% weaker than those of the other two. This value of 5% is much larger than the experimental error. It is commonly assumed that the recoil-free fraction factors are similar for the three Fe sites of BCT Fe_3B and the relative intensities are proportional to the on-site Fe atoms occupancies. This result means that some Fe atoms at the $Fe_{III}(8g)$ are substituted by R atoms. The spectrum of $Y_4Fe_{77.5}B_{18.5}$ cannot be fitted with only four subspectra owing to the existence of the $Y_3Fe_{62}B_{14}$ magnetic phase (figure 5(d)). Since its concentration is very small, only one subspectrum with an average field of 272 kOe is employed to fit this phase. The fitting parameters of $R_4Fe_{77.5}B_{18.5}$ are summarized in table 2.

Figure 6 shows the NMR spectra measured at 8 K for the heat-treated samples. The very weak peak centred at 46.7 MHz is associated with ^{57}Fe nuclei in α-Fe. Since the concentration of α-Fe in these samples is very small (about 5 at.%) and the natural abundance of ^{57}Fe nuclei is only about 2.2%, the ^{57}Fe signal is too weak to be detected by NMR in some samples. In agreement with the XRD and Mössbauer results, the NMR spectra also show that these samples do not contain the hard magnetic phase $Nd_2Fe_{14}B$ (2:14:1).

It is possible that the atomic ordering in the 2:14:1 lattice may be still far from perfect and its grain size is too fine to be resolved by XRD, but both NMR and the ME can obtain information concerning the nearest-neighbour environment of the detected nuclei. When there exists a certain short-range order in the nearest-neighbour B atoms, about 10–100 Å, it can be detected by NMR and the ME. In this way, NMR and the ME can be utilized to identify phase compositions whose dimensions are too small for XRD techniques. On the one hand, although B atoms are not the major component presented in the 2:14:1 phase, the natural abundance of ^{11}B is about 80.8%. Furthermore, zero-field spin-echo NMR signals come primarily from domain walls in a polycrystalline ferromagnetic material and have a larger enhancement factor than those arising from domains. When the 2:14:1 phase appears, ^{11}B NMR signals can be easily detected. For small particles whose sizes are smaller than the critical size of single domains, NMR is more difficult to observe than multi-domain NMR owing to the smaller signal intensity [11], but Mössbauer measurements are not influenced by the difference between a domain and a domain wall. On the other hand, one should note

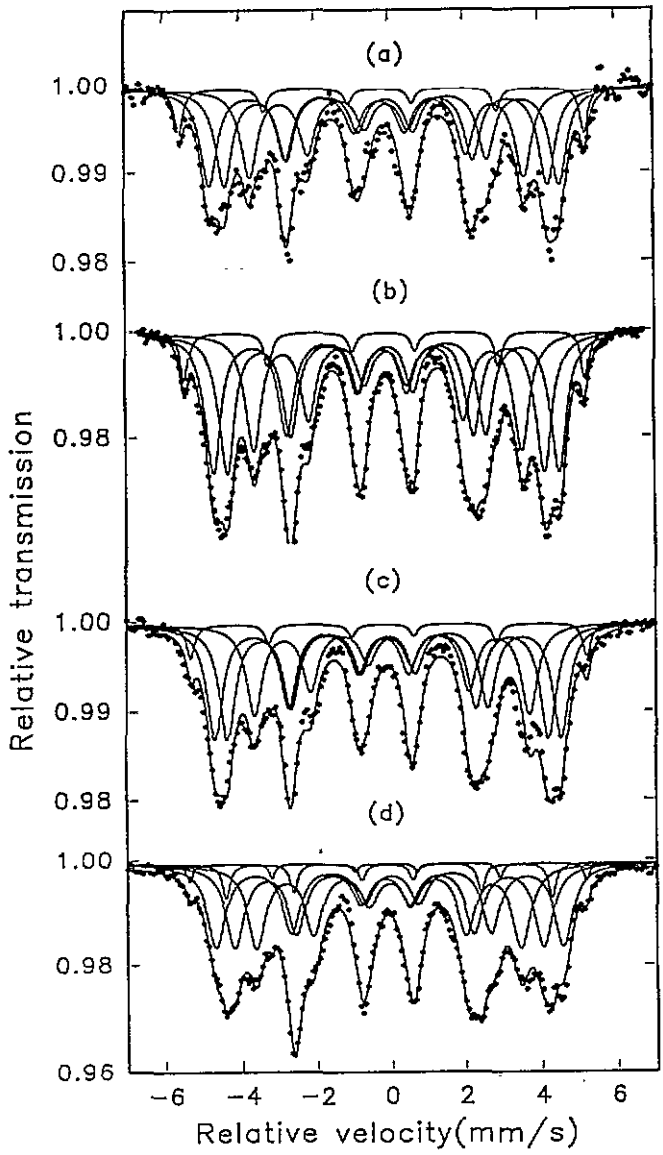

Figure 5. ^{57}Fe Mössbauer spectra of $R_4Fe_{77.5}B_{18.5}$ annealed alloys: (a) R ≡ Pr; (b) R ≡ Nd; (c) R ≡ Gd; (d) R ≡ Y.

that there is a much lower probability that the signal of the $Nd_2Fe_{14}B$ phase overlaps that of BCT Fe_3B. For NMR, the difference between the ^{11}B and ^{57}Fe hyperfine fields in BCT Fe_3B and $Nd_2Fe_{14}B$ is very large. For the Mössbauer experiment, a subspectrum with an average hyperfine field of 301 kOe for $Nd_2Fe_{14}B$ does not appear between the hyperfine field of 333 kOe for α-Fe and the hyperfine field of 288 kOe for the first subspectrum of BCT Fe_3B. Thus, it can be concluded that the 2:14:1 phase is not present in these samples. In our previous work, we ruled out the possibility of the hard magnetic properties originating from the $Nd_2Fe_{14}B$ hard magnetic phase [7, 8].

On the basis of XRD and Mössbauer spectrum results, the intense peaks in figure 5, e.g.

Table 2. Mössbauer fitting parameters of $R_4Fe_{77.5}B_{18.5}$ annealed at 670 °C for a short time.

Samples	Component	Intensity (%)	Linewidth (mm s^{-1})	Isomer shift (mm s^{-1})	Quadrupole shift (mm s^{-1})	Hyperfine field (kOe)
$Pr_4Fe_{77.5}B_{18.5}$	α-Fe	6.5	0.25	0	0.02	333.1
	BCT Fe_3B (I)	32.1	0.52	0.06	0.00	286.0
	(II)	32.1	0.52	−0.01	0.08	264.4
	(III)	29.3	0.52	0.10	0.00	224.9
$Nd_4Fe_{77.5}B_{18.5}$	α-Fe	5.6	0.26	0	0.02	333.2
	BCT Fe_3B (I)	33.2	0.51	0.06	0.00	288.2
	(II)	33.2	0.51	−0.01	0.04	264.2
	(III)	28.0	0.51	0.08	0.02	224.2
$Gd_4Fe_{77.5}B_{18.5}$	α-Fe	4.6	0.26	0	0.08	332.0
	BCT Fe_3B (I)	34.2	0.52	0.06	−0.01	288.3
	(II)	34.2	0.52	−0.01	0.06	265.1
	(III)	27.0	0.52	0.09	0.03	224.1
$Y_4Fe_{77.5}B_{18.5}$	α-Fe	2.2	0.18	0	0.02	330.2
	BCT Fe_3B (I)	30.7	0.59	0.10	−0.02	289.3
	(II)	30.7	0.59	0.01	0.05	257.8
	(III)	30.7	0.59	0.07	−0.02	221.4
	$Y_3Fe_{62}B_{14}$	5.7	0.24	0.03	0.02	271.9

centred at 34.7 MHz for R ≡ Y, Nd and Pr and 36.0 MHz for R ≡ Gd are assigned to the ^{11}B resonance signals in BCT Fe_3B. For the samples with R ≡ Pr and Nd, the strong line centred at 34.7 MHz is the characteristic peak of BCT Fe_3B, but it broadens asymmetrically to the high-frequency side. It is noteworthy that the ^{11}B NMR peaks corresponding to BCT Fe_3B shift from 34.7 MHz (25.3 kOe) to 36.0 MHz (26.3 kOe) with the addition of Gd and Dy.

It is known that both NMR and the ME, the hyperfine interaction techniques, can provide information concerning the local neighbourhood of the resonant nuclei. It can distinguish lattice sites which are magnetically, atomically or electronically inequivalent. For BCT Fe_3B, B atoms are always located in the centre of a trigonal prism formed by the nearest Fe atoms [14]. When there are some fluctuations in the nearest-neighbour B atoms, they are bound to influence the electronic structure of the B atoms and, consequently, change the hyperfine field and its distribution at B sites. For NMR experiments, the change manifests itself in the variety of resonance lines. If the change is significant, the NMR peaks will shift or a new resonant peak will appear. If not, the spectrum will broaden or distort. The fact that the ^{11}B hyperfine field increases with increasing x can be explained by the entry of the R atoms into the BCT Fe_3B. For the sample $Y_4Fe_{77.5}B_{18.5}$, the NMR spectrum shows the peaks located at 34.7 MHz without any distortion, but a new peak centred at about 39.0 MHz appears. This peak may originate from ^{11}B nuclei in the $Y_3Fe_{62}B_{14}$ magnetic phase on the basis of the XRD result. A further study is in progress.

Figure 7 shows the ^{11}B hyperfine field in BCT Fe_3B as a function of the R concentration x, with an approximately linear relationship between the hyperfine field and the R concentration. Since full substitution of Nd by Dy will lead to the appearance of $Dy_3Fe_{62}B_{14}$, only $x = 0$, 1 and 2 are shown for R ≡ Dy. Owing to the non-magnetic B atoms, the contribution to the hyperfine field at B sites in R–Fe–B compounds and/or alloys arises mainly from the transferred hyperfine field. The transferred hyperfine field is proportional to the number of its nearest-neighbour magnetic atoms and their magnetic moments [15].

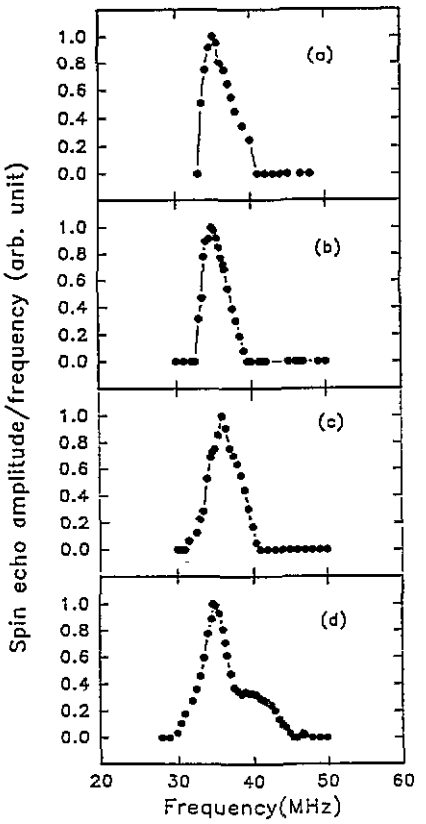

Figure 6. ^{11}B NMR spectra of $R_4Fe_{77.5}B_{18.5}$ annealed alloys: (a) R ≡ Pr; (b) R ≡ Nd; (c) R ≡ Gd; (d) R ≡ Y.

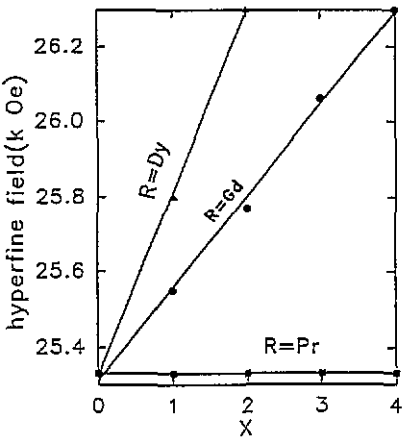

Figure 7. The hyperfine field at B sites in BCT Fe_3B versus the R concentration in $R_xNd_{4-x}Fe_{77.5}B_{18.5}$ alloys.

For the samples with R ≡ Pr, the ^{11}B hyperfine fields obviously show no increase with increasing Pr concentration. This is due to the approximately equal values of the Nd and Pr moments. However, the addition of Gd or Dy will increase the ^{11}B hyperfine fields in BCT Fe_3B owing to the larger moments of Gd and Dy. The coupling between light rare-earth elements, such as Pr or Nd, and Fe is ferromagnetic while that of heavy rare earths, such as Gd or Dy, and Fe is antiferromagnetic, but both light rare-earth substitution and heavy rare-earth substitution increase the hyperfine field at B sites. This means that the contribution of R atoms to the transferred hyperfine field comes from the R magnetic moments of Nd and Gd via the polarization of conduction electrons.

Figure 8 shows the coercive fields H_c of heat-treated alloys containing several mixtures of rare-earth elements. For the samples with R ≡ Pr, the H_c decreases slightly with increasing Pr concentration while, for R ≡ Dy, a small addition of Dy will increase the coercive field, but full substitution leads to a decrease in H_c. This can be explained by the increasing tendency to form the $Dy_3Fe_{62}B_{14}$ phase with a cubic structure. The substitution of Nd by Y and Gd will decrease H_c rapidly. For the rare-earth–iron compounds or alloys, the contribution to the magnetocrystalline anisotropy arises mainly from the rare-earth sublattices. The Gd atoms have non-orbit magnetic moments and Y atoms have a non-magnetic moment and, consequently, no contribution to the magnetocrystalline

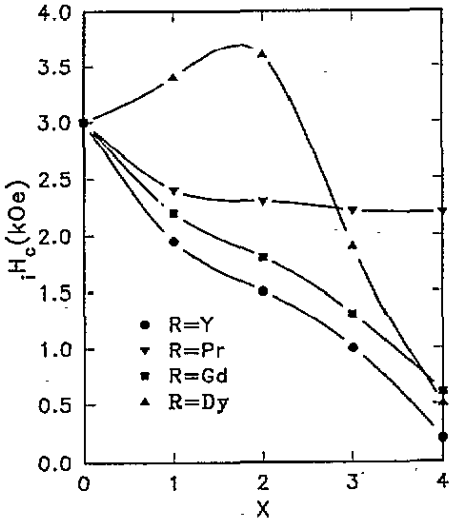

Figure 8. Coercive fields at room temperature of crystallized $R_xNd_{4-x}Fe_{77.5}B_{18.5}$ alloys as a function of R concentration x.

anisotropy. Thus, H_c decreases on the addition of Gd and Y. Hysteresis loops indicate that a characteristic feature of these materials is the high isotropic M_r/M_s ratio of about 0.7–0.8. For an assembly of randomly oriented non-interacting crystallites the uniaxial anisotropy M_r/M_s is 0.5 if the magnetization is determined by a coherent rotation of spin in the grains. The ratio can be even lower owing to domain formation. So the high ratio M_r/M_s or remanence magnetization to saturation magnetization can be explained by the strong magnetic interactions between the uniaxial magnetocrystalline anisotropy of BCT Fe_3B containing R atoms and α-Fe crystallites.

4. Conclusions

(1) The substitution of Nd by R changes the Curie temperatures slightly of amorphous alloys. However, the coercive fields of crystallized alloys decrease with increasing R concentration for R ≡ Y, Pr and Gd. The addition of a small amount of Dy will improve the coercivity, but full substitution of Dy will lead to a decrease in H_c owing to the presence of the magnetically soft phase $R_3Fe_{62}B_{14}$.

(2) The addition of Gd and Dy causes an increase in the ^{11}B hyperfine field in BCT Fe_3B but does not influence that of the α-Fe. This can be explained by the entry of R atoms into the BCT Fe_3B.

(3) The origin of the hard magnetic properties in rapidly quenched Nd–Fe–B with a low Nd concentration is not related to the existence of the 2:14:1 magnetically hard phase, but to the BCT Fe_3B containing Nd atoms.

Acknowledgments

This work was supported by the National Natural Science Foundation of China and the State Key Laboratory of Magnetism, Institute of Physics, Chinese Academy of Sciences.

References

[1] Buschow K H J, de Mooij D B and Coehoorn R 1988 *J. Less-Common Met.* **145** 601
[2] Coehoorn R, Mooij D B, Duchateau J P W B and Buschow K H J 1988 *J. Physique Coll.* **49** C8 669
[3] Coehoorn R, de Mooij D B and de Waard C 1990 *J. Magn. Magn. Mater.* **80** 101
[4] Eckert D, Handstein A, Müller K H, Hesske R, Schneider J, Mattern N and Illgen L 1990 *Mater Lett.* **9** 289
[5] Müller K H, Schneider J, Handestein H, Eckert D and Nothnagel P 1991 *Mater. Sci. Eng.* A **133** 151
[6] Shen B G, Yang L Y, Zhang J X, Gu B X, Ning T S, Wo F, Zhao J G, Guo H Q and Zhan W S 1990 *Solid State Commun.* **74** 893
[7] Mao M X, Yang C L, Cheng Z H, Zhang Y D, Shen B G, Yang L Y and Li F S 1992 *J. Phys.: Condens. Matter* **4** 9147
[8] Cheng Z H, Mao M X, Sun J J, Yang C L, Zhang Y D, Li F S, Shen B G and Zhang J X 1994 *J. Appl. Phys.* **76** 2981
[9] Ge S H, Mao M X, Chen G L, Cheng Z H, Zhang C L, Zhang Y D, Hines W A and Budnick J I 1992 *Phys. Rev.* B **45** 4695
[10] Zhang Y D, Budnick J I, Ford J C and Hines W A 1991 *J. Magn. Magn. Mater.* **100** 13
[11] Dai D S, Fang R Y, Tong L T, Li Z X, Zhou Z J and Lin Z H 1985 *J. Appl. Phys.* **57** 3589
[12] Shen B G, Zhang J X, Yang L Y, Guo H Q and Zhao J G 1991 *Mater. Sci. Eng.* A **133** 162
[13] de Mooij D B, Daams J L C and Buschow K H J 1987 *Philips J. Res.* **42** 3391
[14] Gaskell P H 1981 *Nature* **289** 474
[15] Zalesskij A V and Zheludev I S 1976 *At. Energy. Rev.* **141** 133